Kulikova, G., Schurr, B., Krüger, F., Brzoska, E., Heimann, S. (2016): Source parameters of the Sarez Pamir earthquake of February 18, 1911. - *Geophysical Journal International*, *205*, 2, pp. 1086—1098.

DOI: http://doi.org/10.1093/gji/ggw069

Geophysical Journal International

Geophys. J. Int. (2016) **205,** 1086–1098
Advance Access publication 2016 February 19
GJI Seismology

doi: 10.1093/gji/ggw069

Source parameters of the Sarez-Pamir earthquake of 1911 February 18

Galina Kulikova,[1] Bernd Schurr,[2] Frank Krüger,[1] Elisabeth Brzoska[3] and Sebastian Heimann[2]

[1]*Institute of Earth and Environmental Science, University of Potsdam, K.-Liebknecht-Str.* 24/H60, *D*-14476 *Potsdam, Germany. E-mail: kulikova@geo.uni-potsdam.de*
[2]*Helmholtz Centre Potsdam, GFZ German Research Centre for Geosciences, Telegrafenberg, D*-14473 *Potsdam, Germany*
[3]*Institute of Applied Geosciences, KIT Karlsruhe Institute of Technology, Kaiserstr.* 12, *D*-76131 *Karlsruhe, Germany*

Accepted 2016 February 15. Received 2016 February 14; in original form 2015 September 1

SUMMARY

The $M_s \sim 7.7$ Sarez-Pamir earthquake of 1911 February 18 is the largest instrumentally recorded earthquake in the Pamir region. It triggered one of the largest landslides of the past century, building a giant natural dam and forming Lake Sarez. As for many strong earthquakes from that time, information about source parameters of the Sarez-Pamir earthquake is limited due to the sparse observations. Here, we present the analysis of analogue seismic records of the Sarez-Pamir earthquake. We have collected, scanned and digitized 26 seismic records from 13 stations worldwide to relocate the epicentre and determine the event's depth (∼26 km) and magnitude (m_B7.3 and M_s7.7). The unusually good quality of the digitized waveforms allowed their modelling, revealing an NE-striking sinistral strike-slip focal mechanism in accordance with regional tectonics. The shallow depth and magnitude (M_w7.3) of the earthquake were confirmed. Additionally, we investigated the possible contribution of the landslide to the waveforms and present an alternative source model assuming the landslide and earthquake occurred in close sequence.

Key words: Earthquake source observations; Seismicity and tectonics; Body waves; Theoretical seismology.

1 INTRODUCTION

The Sarez-Pamir M7$\frac{3}{4}$ Gutenberg & Richter (1954) earthquake occurred on 1911 February 18 on the Pamir plateau, northwest of Tibet (Fig. 1). This earthquake is famous for having triggered one of the largest rockfalls on Earth (Ambraseys & Bilham 2012). The Usoy slide, named after the village it buried, blocked the Murgab river and created largest natural dam on Earth (Preobrazhenskiy 1920). The river water started filling up the valley, forming a lake, and by the end of summer 1911 it flooded the Sarez village. Usoy dam and the newly formed Lake Sarez (Fig. 1), named after the lost village, with its 17 cubic kilometres of stored water, have attracted significant attention from the scientific community due to the enormous consequences a possible breach would entail (Papyrin 2001; Kazakov 2004; Ischuk 2006).

The extent of the Usoy catastrophe was not immediately known to the local government, nor was the time of occurrence of the Usoy landslide with respect to the Sarez earthquake (Shpilko 1914). The earthquake and the landslide had destroyed the mountain paths to the district centre, interrupting efficient communication and the first information about the catastrophe and rising lake was only received 45 d after the event. When the first commission investigated the lake, oral testimonies stated that the landslide and the earthquake happened at approximately the same time. The fact that the level of Lake Sarez was rising was confirmed and the Sarez villagers were evacuated and relocated. The village was completely flooded by mid-Autumn 1911 (Shpilko 1914).

The first expedition of Preobrazhenskiy was sent to Lake Sarez in 1915 to perform mapping, geological and geodetic surveys. They estimated the volume (2.2 km^3) and the mass (6×10^{12} kg) of the landslide and their work 'Usoy avalanche' (Preobrazhenskiy 1920) was published in 1920. These data remain relevant to the present day.

In comparison to the landslide, the Pamir-Sarez earthquake itself attracted less attention from the scientific community until 1915, when Galitzin expressed the idea that there was no earthquake at all and that it was the landslide that was registered on the seismic records (Galitzin 1915). Based on the data of Preobrazhenskiy (1920), Galitzin (1915) calculated the potential energy released by the landslide and concluded that it would be sufficient to produce the seismic amplitudes recorded on the Pulkova seismic station ∼3800 km away. This idea created a long dispute among seismologists at the time, either agreeing (Klotz 1915; Jeffreys 1923) or disagreeing (Oldham 1923; Jeffreys 1924) with Galitzin's suggestion.

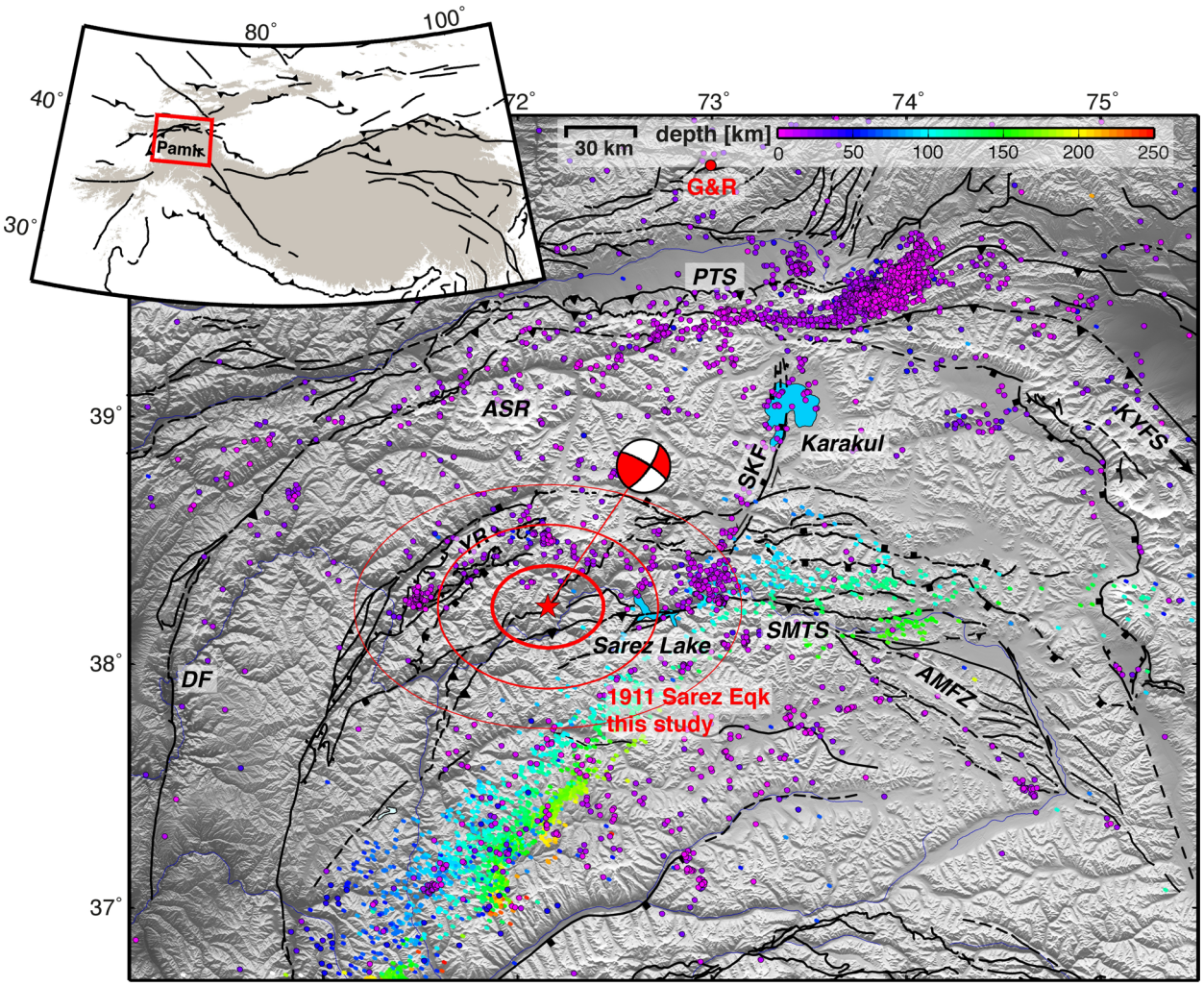

Figure 1. Seismicity map of the Pamir region. Epicentres (Sippl *et al.* 2013b) are colour-coded by depth. Major faults from Schurr *et al.* (2014) are shown as black lines. The red circle marked as G&R indicates the epicentre of the 1911 Sarez-Pamir earthquake from Gutenberg & Richter (1954). The red star and beachball indicate the epicentre and double-couple source mechanism for the 1911 earthquake were derived in this study. The geological structures and geographic names mentioned in the text are abbreviated as follows: SKF—Sarez-Karakul Fault; DF—Darvaz Fault; PTS—Pamir Thrust System; AMFZ—Aksu Murghab Fault Zone; SMTS—Sarez Murghab Thrust System; KYFS—Kashgar-Yecheng Fault Systems; ASR—Academy of Science range. Inset map (top left) shows the location of the study region within the India-Asia collision zone (approximated by shaded region with altitude higher than 2500 m) with the study area shown as a red box.

Oldham (1923) stated that the existence of aftershocks suggested an earthquake source, as does the damage and intensity distribution, which he argues was more typical for a deeper earthquake (relative to a surficial impact). More recently, Ambraseys & Bilham (2012) showed that the landslide would probably not be recorded the same way as an earthquake at teleseismic distances due to its much longer source duration. Although it has been convincingly argued by Ambraseys & Bilham (2012) that there was an earthquake, its source parameters, that is, hypocentre and mechanism, are highly uncertain or completely unknown. Being the largest known event in the region, this information is of particular interest to assess regional tectonics.

We have collected historical seismograms and bulletins for the Sarez-Pamir earthquake to learn more about this exceptional event. We scanned and digitized the analogue seismic records and used them together with bulletin information to locate its epicentre and determine its magnitude and depth. Furthermore, we employed waveform modelling to determine the focal mechanism, centroid depth and the seismic moment of the earthquake. Additionally, we compared the waveforms with the ones from the recent 2015 December 7 M7.2 Tajikistan earthquake in order to check whether the source parameters are similar. Finally, based on examples of modern large landslides, we modelled the Usoy landslide waveforms and investigated how it could have been recorded on the analogue teleseismic records.

2 TECTONIC SETTING

The Pamir mountains, located northwest of the Tibetan plateau, are part of the India-Asia collision zone (Fig. 1). The Pamir crust consists of several terranes that amalgamated on the southern margin of Asia during the late Palaeozoic and Mesozoic (Burtman & Molnar 1993; Schwab *et al.* 2004). During the Cenozoic collision with India, this crustal package was shortened, reactivating the old sutures as thrust faults and displaced northwards in front of the advancing Indian plate promontory (Burtman & Molnar 1993). Northward displacement was accommodated by strike-slip systems on the flanks of the orogene. In the west, the active sinistral

Darvaz fault separates the Pamir from the Tajik basin. In the east, the dextral Karakorum and Kashgar-Yecheng fault systems presumably translated the Pamir along the western margin of the Tarim basin (Fig. 1). Currently, the Pamir and Tarim basin move at approximately the same speed, rendering these shear zones mostly inactive (Sobel *et al.* 2011). Significant syn-tectonic extension is documented in the Pamir plateau by the exhumation of several gneiss domes (Robinson *et al.* 2004; Stübner *et al.* 2013a). North–south extension ceased in the last 2 Ma (Stübner *et al.* 2013b), but east–west extension is still active (Robinson *et al.* 2004; Zubovich *et al.* 2010; Ischuk *et al.* 2013).

In the current deformation regime, shortening is localized across Pamir's northern margin at a rate of approximately 1.5 cm a^{-1} (Zubovich *et al.* 2010; Ischuk *et al.* 2013). It is accommodated by thrust faulting across the Pamir Thrust System (Schurr *et al.* 2014), with the 2008 M6.7 Nura event being the most recent of such events (Sippl *et al.* 2014; Teshebaeva *et al.* 2014). In the Pamir interior, where the Sarez-Pamir earthquake presumably occurred, sinistral strike-slip faulting prevail on northeast trending or conjugate planes and to a lesser degree north–south striking normal faulting, indicating east–west extension and north–south shortening (Schurr *et al.* 2014; Fig. 1). This pattern has been corroborated by the very recent 2015 M_w 7.2 Sarez-Pamir earthquake (Fig. 1). In contrast, the long term, mostly east–west striking Cenozoic geological structures, recording both thrusting and normal faulting, are largely inactive (Fig. 1). This change in the deformation regime is presumably young, and has not yet left its imprint in the structural grain. The only recent fault system striking NE and exhibiting sinistral trans-tension in the Central Pamir, which is visible both in the landscape and in the seismicity pattern, is the Sarez-Karakul fault system (Strecker *et al.* 1995; Schurr *et al.* 2014). It strikes NE from Lake Sarez across Lake Karakul to reach the Pamir thrust system (Fig. 1). Its surface morphology exhibits an echelon, right-stepping escarpments, with oblique faults, having both sinistral strike-slip and normal displacements, also indicated by offset stream channels, fault slip data and recent scarps (Strecker *et al.* 1995; Schurr *et al.* 2014). It is traced by seismicity, with the few available mechanisms indicating sinistral strike-slip faulting (Schurr *et al.* 2014), and the recent large 2015 M_w 7.2 event might have occurred on it. This fault system seems to roughly separate the stable eastern Pamir from the seismically more active western Pamir. The current deformation is thought to reflect gravitational collapse and westward extrusion of Pamir rocks under north–south compression (Schurr *et al.* 2014). The east–west extension indicated by Pamir earthquake fault mechanisms and GPS vectors is balanced by east–west shortening in the Tajik basin (Ischuk *et al.* 2013).

The Pamir also features an intermediate depth (~80–240 km) seismic zone, which is very rare in continental settings (Sippl *et al.* 2013b). The earthquakes form a tight 90° arc (Fig. 1) and apparently trace Asian lithosphere subducting under the Pamir (Burtman & Molnar 1993; Sippl *et al.* 2013a; Schneider *et al.* 2013).

3 SEISMOGRAM COLLECTION AND DIGITIZATION

By the beginning of the 20th century, seismographs developed by the early seismologists—Rebeur-Paschwitz, Ehlert, Wiechert, Omori, Milne, Galizin, etc. (Milne 1886; Ehlert 1898; Omori 1899; Wiechert 1903, 1904; Galitzin 1910; Fréchet & Rivera 2012)—were already deployed in observatories worldwide, together forming the first seismic network. However, distribution of the observatories was quite heterogeneous with, for example, clustering in Europe and emptiness in Africa (Batlló *et al.* 2008), causing large observational azimuthal gaps for many earthquakes, including the Sarez-Pamir earthquake (Fig. 2). Early seismic instruments were mainly one- or two-component horizontal seismometers functioning as mechanical pendulums (e.g. Wiechert, Bosch-Omori, Vicentini, etc.), but the first electromagnetic seismic instruments (Galitzin 1910) were also already installed in some observatories. Each instrument was characterized by its own free period, damping and magnification values (Table A1, Supporting Information). Before radio timing signals became available in the 1920s, the timing of early analogue seismographs was done using local astronomical clocks, introducing significant uncorrelated errors across stations and networks. Vertical component seismographs were developed only later (in 1905, Dewey & Byerly 1969) and added as separate instruments afterward (mostly after 1910, Wood 1921; McComb & West 1931). The pendulum-type seismographs were typically constructed with a needle fixed on an approximately 45 cm long metal arm attached to a moving mass, which recorded the ground motion by scratching on smoked paper fixed on a rotating cylinder.

The 1911 Sarez-Pamir earthquake must have been recorded by many seismic stations worldwide, but collecting those seismic records today is difficult. Many seismograms probably did not survive and those which still exist are scattered in local archives of different observatories (Batlló *et al.* 2008). Collecting these entails visiting each archive individually, which is complicated due to the necessity for extensive travel and the need of powerful onsite scanning facilities. Nonetheless, in a significant effort we have collected 60 seismograms from 25 different seismic stations for the Sarez-Pamir earthquake. Forty of those records were obtained from the National Institute of Geophysics and Volcanology (INGV) in Rome, Italy, which is a great source for historical seismograms from European seismic stations. These records had been collected by INGV in Rome within the EUROSISMOS project (Michelini *et al.* 2005). Other seismograms were obtained by personal contact to different local institutes (see Table A1, Appendix A in the Supporting Information for details).

The paper seismograms were scanned with high resolution, keeping their original size, to be able to later extract the true amplitudes. Obtaining reliable digital seismograms from those scanned records is a challenging procedure. The Sarez-Pamir earthquake was mainly recorded on old smoked paper, which does not allow an automatic digitizing procedure. Consequently, the seismograms were digitized manually using the path tool of GIMP (GNU Image Manipulation Programme; Kimball *et al.* 2014) by basically retracing them. The GIMP output path was then smoothed using Bezier curves, resampled with a constant sampling rate of 0.1s and converted to ASCII text format. The pendulum seismographs introduce a curvature to the waveform registration, which is particularly obvious for large oscillations (Fig. 3). We corrected for curvature using the method of Cadek (1987) and Grabrovec & Allegretti (1994).

Eventually we were able to digitize 26 seismograms from 13 seismic stations. Eleven of those stations were located in Europe (Fig. 2), one station in Japan and one in Indonesia. This leaves large azimuthal gaps of about 180° in the SE-NW quadrants and about 90° in the N-NE quadrant. However, the dense network in Europe allows using these stations as a large aperture seismic array to align and stack the records for further analysis. The European seismic stations were equipped with Wiechert seismographs and generally provided good quality records with clear P, S and surface waves. An example of a Wiechert record from a European station—MNH (Munich, Germany)—is shown in Fig. 3. The Dutch station DBN,

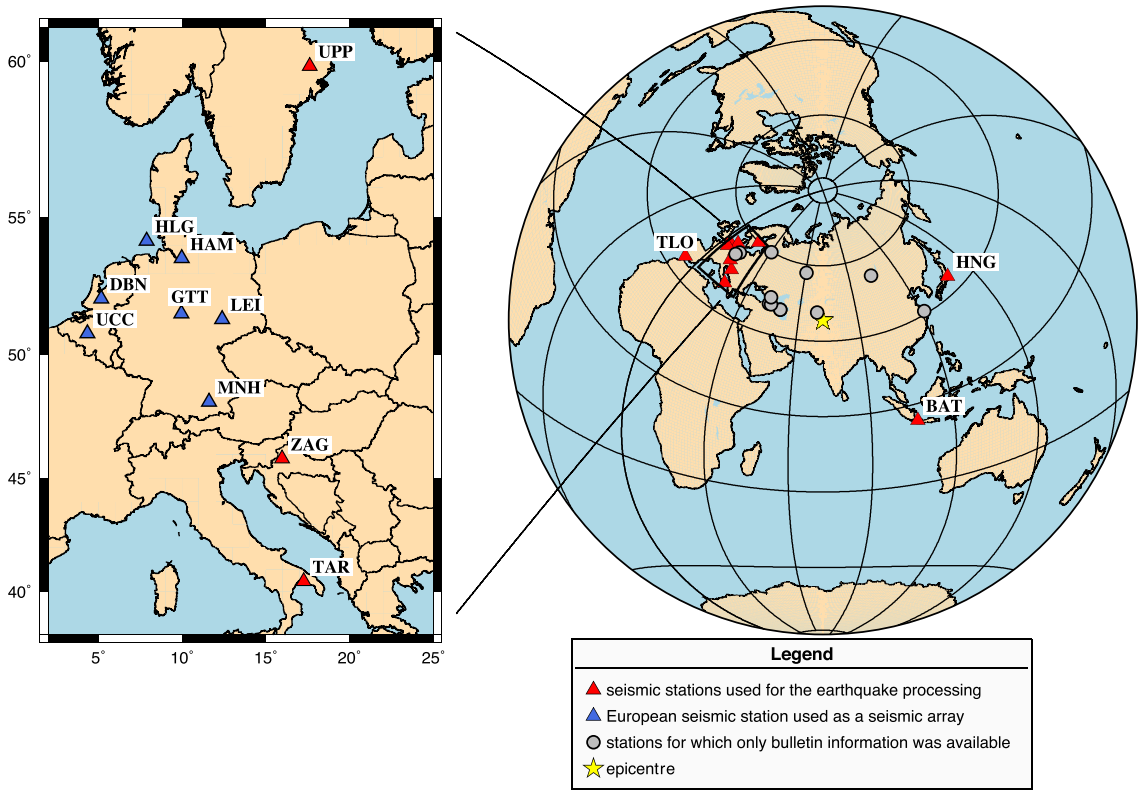

Figure 2. Seismic stations that have recorded the Sarez-Pamir earthquake. The star in the middle represents the earthquake epicentre; red triangles show the stations which were used in this study with corresponding station abbreviation names (the station abbreviations are given according to the name of the nearest modern station); the grey circles show the stations for which only bulletin information was available. The inset map (left side) shows the seismic station distribution in Europe: blue triangles mark the stations used as a seismic array, red triangles mark other stations.

in addition to the Wiechert seismograph, and the Japanese station HNG were equipped with Bosch–Omori instruments. Their low magnification of only 20 prevented reading the P arrival. The station BAT in Indonesia provided only a north–south component record, which was very oscillatory, probably due to specific site conditions and low damping. Nonetheless all phases could be identified at this station.

4 EARTHQUAKE LOCATION AND MAGNITUDE

4.1 Earthquake relocation

Previous studies reported quite varying epicentre locations, depths and magnitudes for the Sarez-Pamir earthquake (Fig. 4). Gutenberg & Richter (1954) suggested the epicentre 200 km north of Lake Sarez in the Tian Shan's Alai range, that is, outside the Pamir proper (Fig. 1). The earthquake was later relocated by more authors; Kondorskaya *et al.* (1982) suggest the epicentre exactly at the eastern edge of Lake Sarez based on the macroseismic data of Shpilko (1914) and Galitzin (1915), which then also appears in Kalmetieva *et al.* (2009). Bindi *et al.* (2014) found alternative epicentres based on two different macroseismic data sets (Semenov & Semenov 1958; Ambraseys & Bilham 2012) with a calibrated attenuation model. The ISC GEM catalogue (Storchak *et al.* 2013) locates the epicentre close to the northern edge of Lake Sarez based on arrival times from seismic bulletins. More recently, Ambraseys & Bilham (2012) suggested a location about 30 km west from the ISC GEM epicentre (Fig. 4).

We relocated the epicentre of the 1911 Sarez-Pamir earthquake using both bulletin information and arrival times read from the digitized seismic records. Bulletin times from eight regional Russian seismic stations between 3° and 26° were gleaned from Nikiforov (1912). In addition, bulletin arrival times from six teleseismic stations (distance from 34° to 47°) were used. Due to the presumably large absolute timing errors of the old seismographs, we used arrival time differences whenever possible with preference. In total we have used 9 absolute times (from digitized records) and 65 arrival time differences. Details on all phase arrivals used are given in Table A3, Appendix A (Supporting Information). For inversion, we used the HYPOSAT software (Schweitzer 2001, 2012) with a modified crustal structure based on the CRUST 5.1 model (Mooney *et al.* 1998) and the global velocity model IASPEI91 (Kennett & Engdahl 1991).

The large timing errors in historical seismograms and sparse and uneven station distribution cause large uncertainties in the location. Fortunately, the occurrence of the M_w 7.2 earthquake near Lake Sarez on 2015 December 7, during the work on this manuscript, helped us to test and tune our relocation procedure. This event was very close to Lake Sarez and should be well constrained by the global seismic network (e.g. 269 phase time readings for the USGS location, 6.1 km horizontal and 1.8 km vertical standard errors). Still, epicentre locations and depths from, for example, the USGS and Geofon agencies differ by as much as 33 and 11 km, respectively, that is, more than their standard errors, providing another measure of uncertainty beyond reported error ellipses. The 1911 and 2015 earthquakes have very similar waveforms (see Fig. A6 in the Supporting Information for details) indicating close

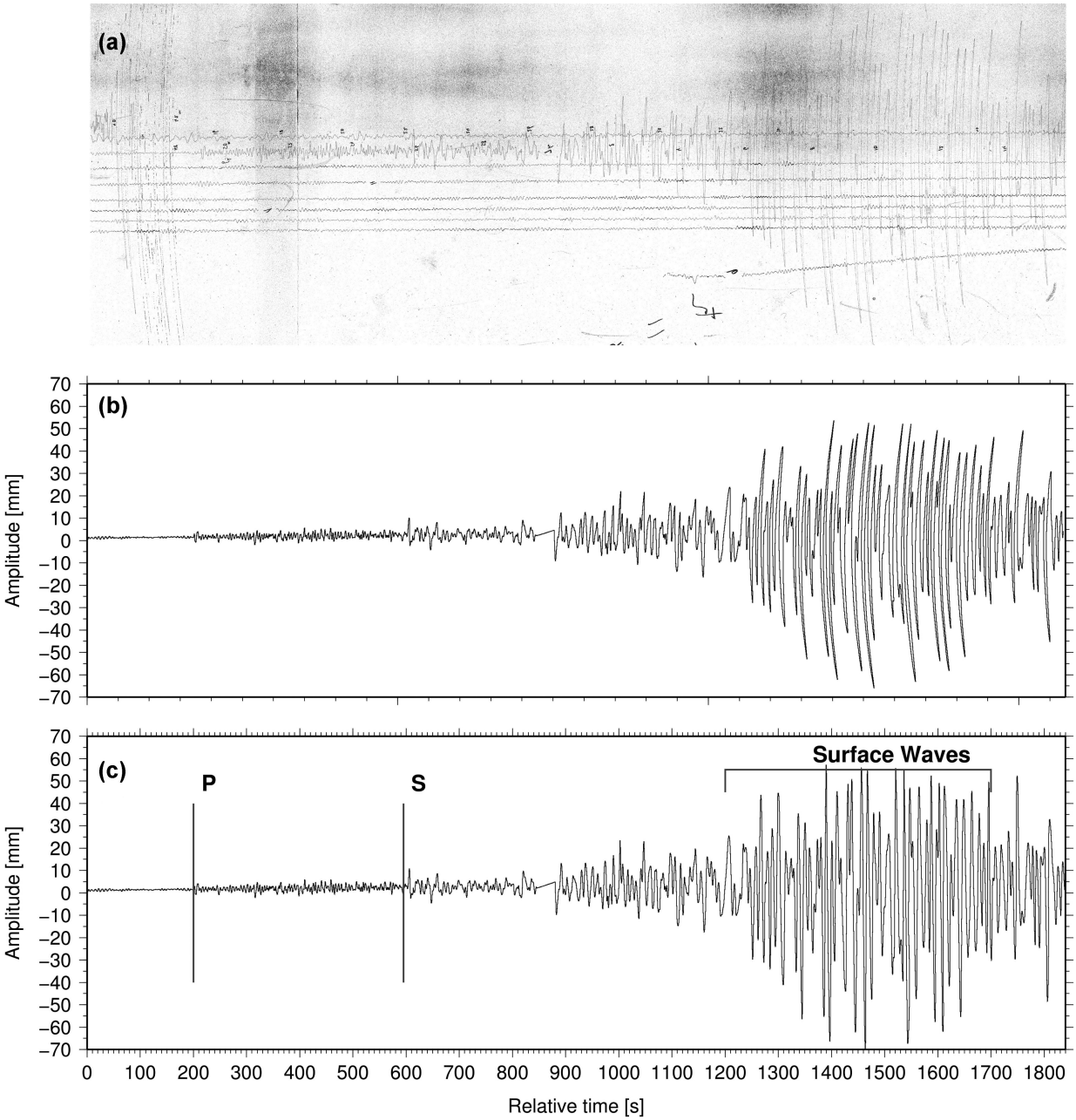

Figure 3. Example scan (a) of the digitized seismogram before (b) and after (c) curvature correction for the East component of the Munich (MNH), Germany, station.

hypocentres. In order to test our location method, we have relocated the 2015 event using a comparable station-phase data set as was available for the 1911 event. This places the 2015 earthquake epicentre about 25 km northeast of its catalogue position (GFZ 2015; USGS 2015; Fig. 4), revealing the bias due to event-station geometry. We then used as a master event, that is, took the Geofon location as fixed, forward calculated traveltimes to stations at or close to historical sites used for the 1911 event and calculated the residuals with respect to the observed traveltimes. These were then used as static corrections for the 1911 event relocation in order to get its position relative to the 2015 event.

As a result (Table 1), the hypocentre of the 1911, Sarez-Pamir earthquake was located at 38.231°N, 72.157°E and 26 km depth (Fig. 4). Standard errors are still large with the long axis of the error ellipse ($1 \times \sigma$) reaching 50 km length (Fig. 1) and a depth error of 14 km. The error ellipse covers the epicentre proposed by Ambraseys & Bilham (2012) and is in good agreement with the intensity distribution map (Ambraseys & Bilham 2012; Fig. 2).

4.2 Magnitude calculation

The reported magnitudes of the Sarez-Pamir earthquake range from M7.1 in (Kalmetieva *et al.* 2009, calculated from regional seismic observations) to M7$\frac{3}{4}$ given by Gutenberg & Richter (1954) and confirmed as M_s7.7 by Ambraseys & Bilham (2012). Intensity based magnitudes calculated by Bindi *et al.* (2014) are $MI_{LH} = 7.4$, $MI_s = 7.6$ and $MI_w = 7.2$.

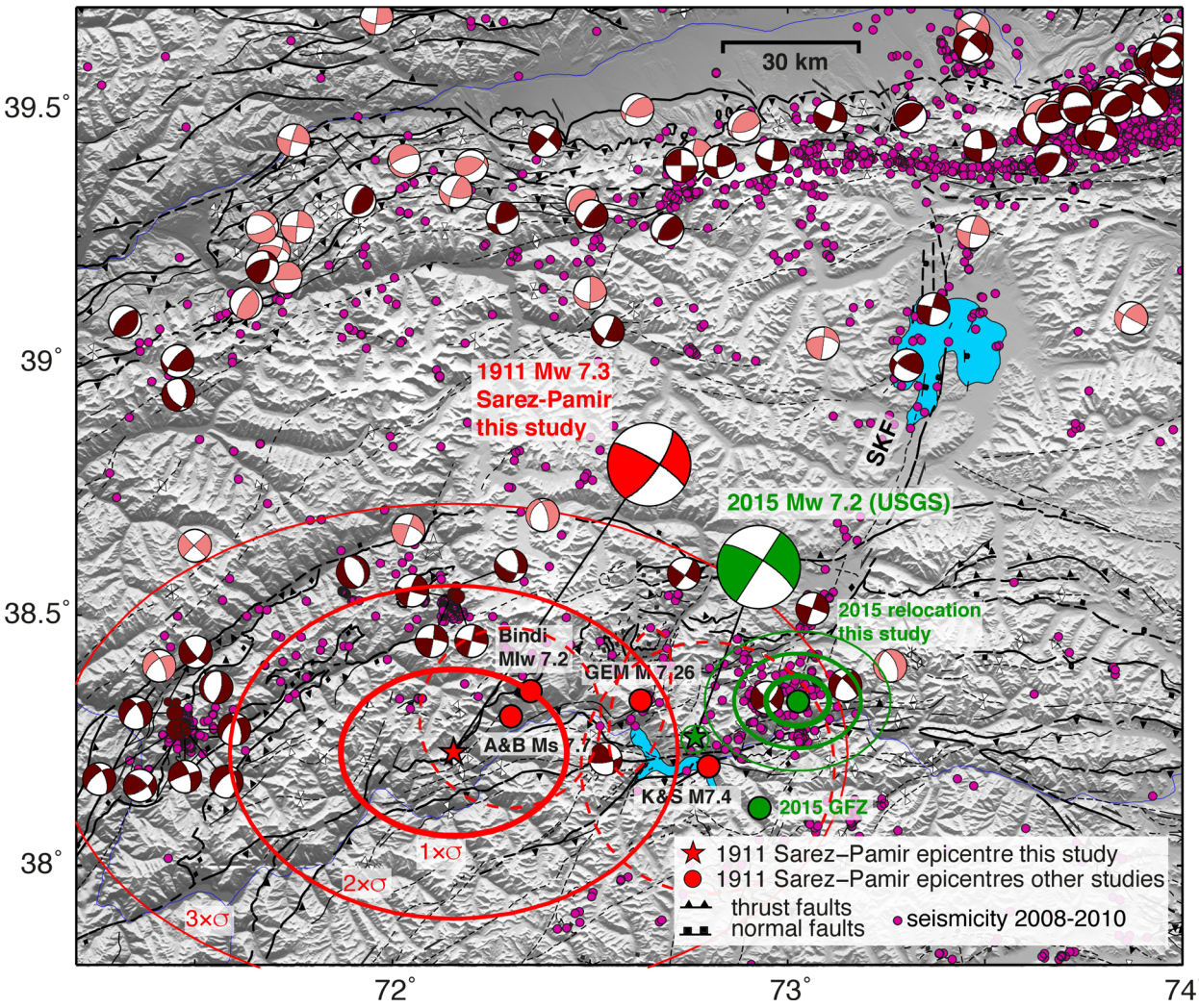

Figure 4. Topographic map of the Sarez-Pamir source region showing focal mechanisms of the global CMT catalogue (Ekström *et al.* 2012) as light red beachballs. Focal mechanisms determined in Schurr *et al.* (2014) are shown as brown beachballs; our epicentre of the 1911 Sarez-Pamir earthquake is represented as a red star, with corresponding 1, 2 and 3 times sigma error ellipses, and the focal mechanism as a red beachball. The epicentres of the 1911 Sarez-Pamir earthquake determined in other studies are shown as red circles named accordingly: Bindi, MI_w7.2—Bindi *et al.* (2014); K&S, M7.4-Kondorskaya *et al.* (1982); Kalmetieva *et al.* (2009); A&B, M_s7.7—Ambraseys & Bilham (2012); GEM, M7.26—Storchak *et al.* (2013). Green star and beachball is the solution for the 2015 Sarez-Pamir earthquake from USGS, green circles are other epicentre solutions for this earthquake.

Table 1. The instrumental epicentre location for the Sarez-Pamir earthquake.

	Origin time (hh:mm:ss.s)	Latitude (°N)	Longitude (°E)	Depth (km)
Preferred location	18:40:58.137 ± 4.768	38.231 ± 0.4460	72.157 ± 0.3344	26.07 ± 14.6

The magnitude M_s7.7 was calculated from amplitudes and periods of surface waves reported in seismic bulletins from worldwide seismic stations (for more details see Ambraseys & Bilham 2012) using the Moscow–Prague formula (Karnik *et al.* 1962). We had some original copies of these bulletins published in Schweitzer & Lee (2003) at hand and, in addition, the surface wave amplitudes measured on the digitized waveforms (Table A4, Appendix A, Supporting Information). We also measured surface wave amplitudes for periods between 18 and 22 s and confirmed the surface wave magnitude M_s7.7 ± 0.1 using the Moscow–Prague formula.

Additionally, the broad-band body wave magnitude m_B (Bormann & Saul 2009; Bormann *et al.* 2013) was calculated using amplitudes and periods of teleseismic body waves. From the bulletin information only this yielded m_B7.1 ± 0.2, while the amplitudes measured on the digitized waveforms resulted in m_B7.3 ± 0.2 (Table A3, Appendix A, Supporting Information), which agrees well with the m_B published by Ambraseys & Bilham (2012) based on their teleseismic bulletin information.

5 FOCAL MECHANISM DETERMINATION

Determination of the focal mechanism for a historical earthquake using standard procedures such as, for example, moment tensor inversion, is not straightforward for a number of reasons (Kulikova & Krüger 2015):

(i) The data quality of digitized seismograms is generally low, often exhibiting steps and kinks from writing-needle dislocations

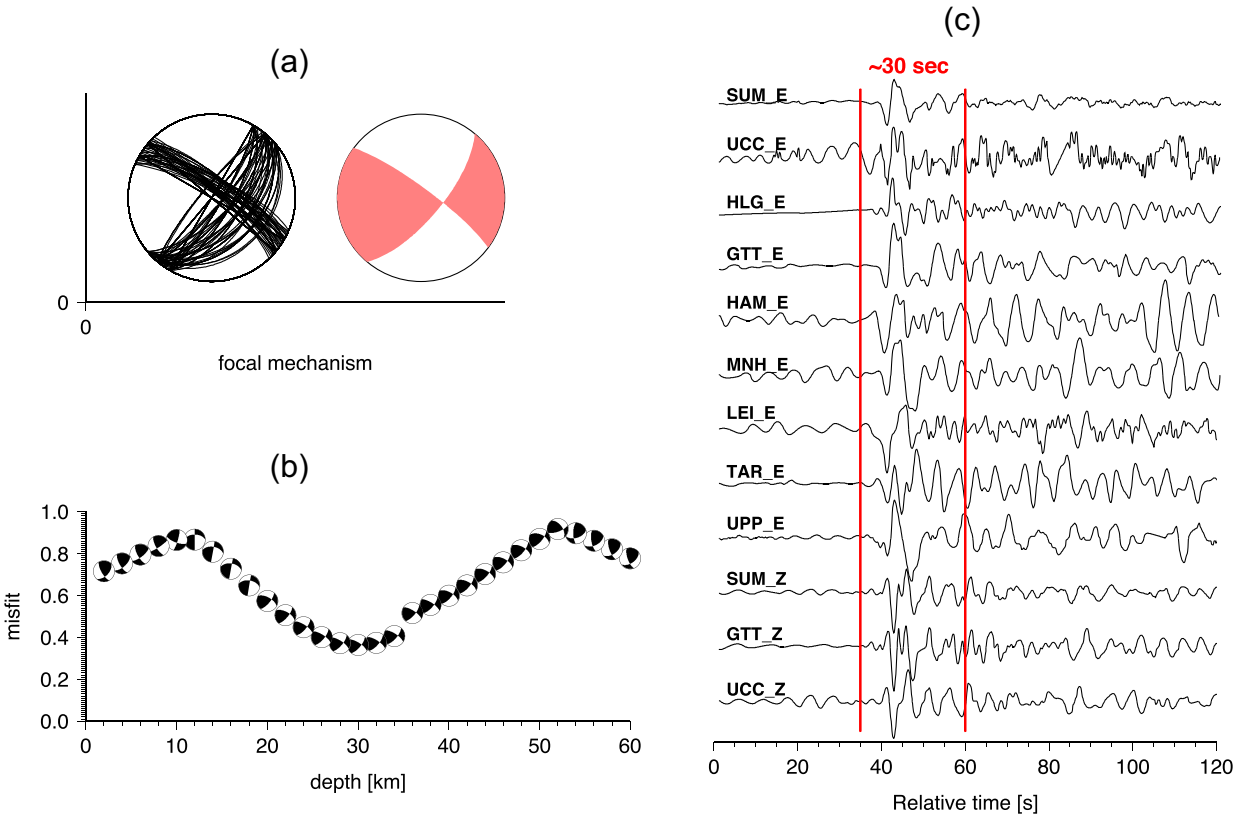

Figure 5. The results of the focal mechanism grid search. (a) The best 5 per cent solutions (left), the light red beachball (right) shows the focal mechanism with the smallest misfit. (b) Misfit function dynamics for the depth of the earthquake, showing a minimum for the depths between 26 and 34 km. (c) The *P* wave records with corresponding station and component name. The solid grey lines mark the *P*-wave duration and hence an estimate of the source duration as ∼30 s. The records are normalized in amplitudes and aligned in time.

leading to interpolation problems when digitizing. These steps introduce artificial low frequencies to the recorded true ground displacement, which can bias moment tensor inversion severely.

(ii) Single horizontal components may be lost and vertical components were, in practically all cases, not yet installed in 1911.

(iii) Imperfect time alignment between different components of the same station hamper the rotation procedure into radial and transverse components.

(iv) The documented instrument parameters (free period, damping and magnification) sometimes do not fully correspond to the real values, which then biases the restitution to true amplitudes of the seismic records.

Due to the above listed factors, we decided to avoid the rotation and restitution of the historical seismic records. Instead, the focal mechanism was determined by fitting the original waveforms to the synthetic seismograms convolved with the historical instrument response in the Z-N-E coordinate system. The Green's functions were calculated with the reflectivity method (Fuchs & Müller 1971; Heimann 2015a) for different test depths (2–60 km, 2 km steps) for all stations using the IASPEI91 velocity model (Kennett & Engdahl 1991) and origin time determined above (Table 1). The synthetic seismograms were calculated for a double-couple (DC) point source for all strike, dip and rake angle combinations with a step of 1° and compared to the observed ones. The best fitting (in a least-squares sense) mechanism and depth were then determined by a grid search.

The free period of the historical instruments varied between 4 and 20 s, which is below or in the range of the corner period of an M7 earthquake. Nonetheless, the body waves were clearly recorded on all the stations except for those two equipped with the Bosch-Omori instrument, due to the low magnification factor of these instruments. However, these two stations provided good quality records for long-period surface waves due to their longer free period (∼20 s). The European stations, mainly equipped with the Wiechert instrument, also clearly recorded the surface waves, even those equipped with very short period instruments (free period between 4 and 7 s, e.g. TAR, BAT, GTT_Z and UCC_Z).

The frequency content of the body waves better fits the pass-band of the historical instruments than that of the surface waves. Nevertheless, we tried to invert for both wave types, and did the inversion for the body waves in the 10–50 s and for the surface waves in the 30–100 s period band. The surface wave inversion did not provide an acceptable solution. The misfit function had a very low dynamic range and a mechanism could not be determined unequivocally. The same situation was observed for the joint inversion of surface waves and body waves, because the solution is dominated by surface waves due to their dominant amplitudes. Consequently, we decided to finalize our inversion based on body waves only. The best waveform fit was found for a focal mechanism with strike/dip/rake: 35°/73°/12° and $M_0 = 8.9 \cdot 10^{19}$ N m, M_w7.3 at 30 km depth (Fig. 5). Being able to fit the waveforms well with a DC source eliminates the last doubts, whether there was an earthquake or not. A first

Sarez-Pamir earthquake

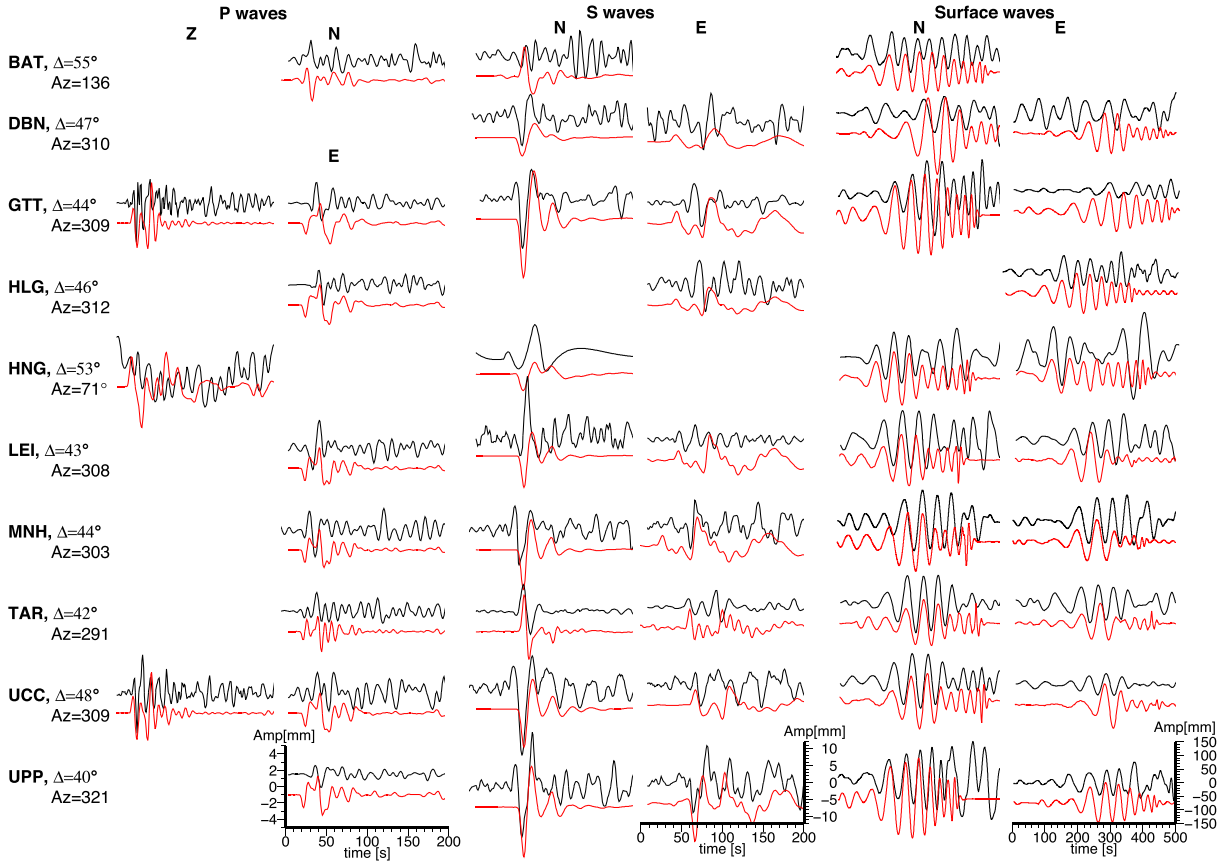

Figure 6. Synthetic and observed waveforms for the 1911 Sarez-Pamir earthquake. The plot shows the synthetic (red lines) and observed (black lines) data for *P* on Z and E components and *S* and surface waves (low-pass filtered, 20 s) on N and E components. The station names are given on the left with corresponding distance (Δ) to the epicentre and the azimuth (Az) in degrees. Amplitude (millimetre on paper) and time (in seconds) scales are given for a few traces as reference, all other traces are on the same scale.

estimate of the source duration of the Sarez-Pamir earthquake could be obtained from the duration of *P* waves on teleseismic records. *P*-wave records for E and Z components of European stations (Fig. 5c) were aligned and stacked, showing that the source duration does not exceed 30 s, which is reasonable for a M_w7.3 earthquake.

The misfit function reveals that the dip and rake angles of the DC are determined rather well within ± 10° precision. However, the strike seems less well resolved showing a lower dynamic range of the misfit function compared to the dip and rake (see Fig. A1 in the Supporting Information for details). The best 5 per cent of the solutions for the focal mechanism (Fig. 5a) show significant variability for the strike. This is probably due to the poor station distribution and thus we give the strike an error estimate of ± 30°. The waveform fit (Fig. 6) is good for body waves with amplitudes and phase matching well. The first onset polarity of the SH waves seems to be reversed for some stations (Fig. 6), which, however, might be a misinterpretation of presiding noise as the first arrival. Although surface waves were excluded in the inversion, the body wave mechanism also shows a good waveform fit for the surface waves (Fig. 6).

6 USOY LANDSLIDE

From our analysis, it is now clear that the seismograms of the 1911 Sarez-Pamir event are dominated by an earthquake. However, some questions on the role of the landslide remain. Ambraseys & Bilham (2012) suggested that the landslide could not have been recorded on distant seismic stations because its energy must have been released over a longer time (they suggest at least ∼3 times the earthquake source duration), leading to considerably smaller amplitudes on seismograms compared to the earthquake signal. Additionally, this low-frequency signal would have been further damped in the records due to the short-period nature of the historical instruments. Here, we try to quantify the possible contribution of the Usoy landslide to the recorded seismograms by modelling its source on simulated historical instruments.

The geological studies (Preobrazhenskiy 1920; Ambraseys & Bilham 2012) estimated the parameters of the landslide quite well, and thus it could be modelled as a sliding rock mass. Its weight was estimated to be about 6×10^{12} kg and the slope angle was between 9° and 20°. In addition Ambraseys & Bilham (2012) estimated the source duration to be ∼107 s and the landslide velocity about 31 m s^{-1}.

It has been shown (Brodsky *et al.* 2003; Moretti *et al.* 2012; Allstadt 2013; Yamada *et al.* 2013) that a landslide signal can be simulated as a combination of a vertical and horizontal single force applied to the ground. We parametrized the force model following Zhao *et al.* (2015), calculating the EW and NS components of the horizontal single force from the strike of the sliding direction. The rest of the Usoy landslide parameters were then used for the

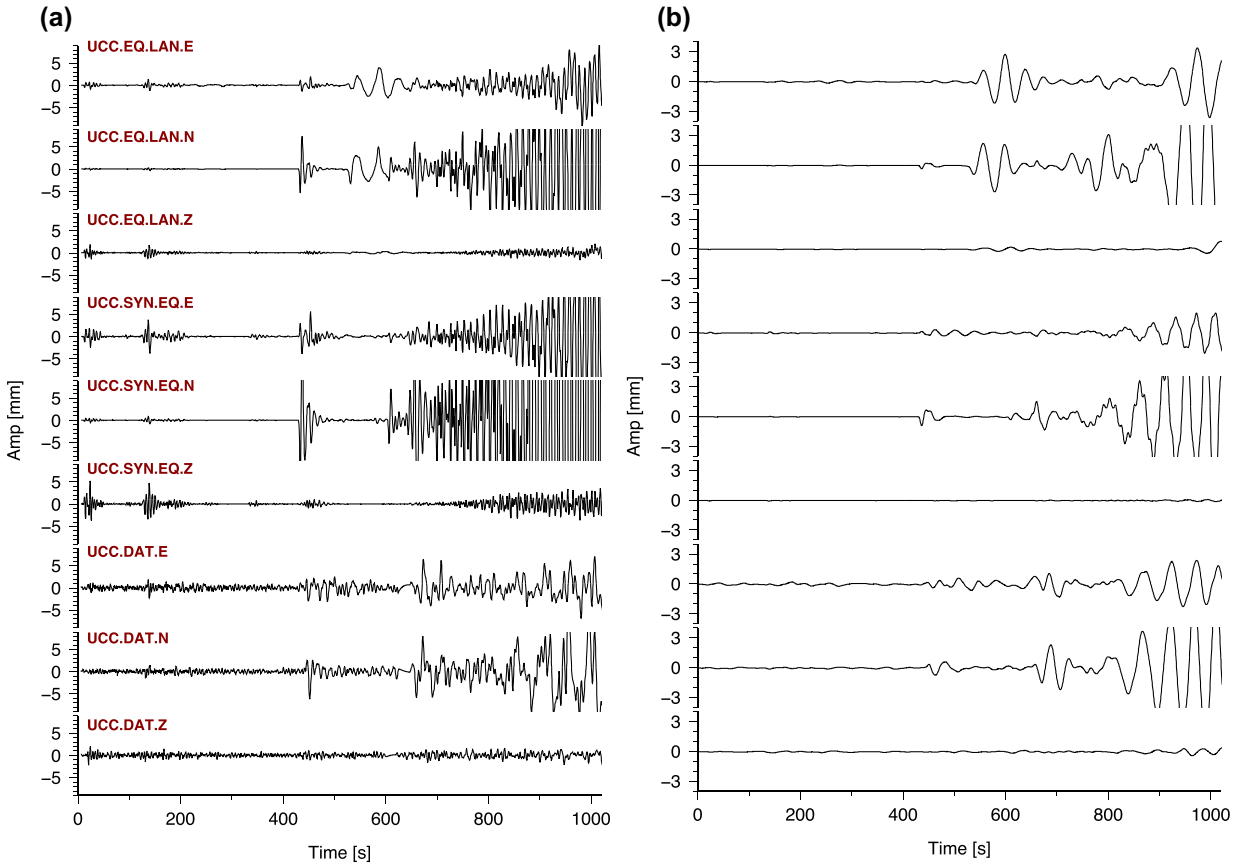

Figure 7. (a) Observed seismograms from the station UCC (Uccle, Belgium) for the 1911 Sarez-Pamir earthquake (DATA) and synthetic waveforms for a double-couple (DC) source (SYN.EQ) and a combination of a DC source and a landslide source (EQ.LAN). The seismograms are not filtered and not normalized. The amplitudes Amp[mm] are given in millimetres on paper record. (b) Same as (a) but low-pass (40 s) filtered.

calculation of the Green's functions. These were then convolved with the instrument responses to produce synthetic seismograms (Heimann 2015a,b).

This scenario produces about 0.4 mm ground displacement for a station located in Europe (distance ∼45°) which, in turn produces an amplitude of about 2.5 cm on a Wiechert seismograph at the GTT station (Göttingen, Germany, magnification 20–50 for long periods) for the surface waves (see Fig. A2, in the Supporting Information). For the Bosch–Omori instrument located in Japan (seismic station HNG) with a magnification factor of 20, the recorded pulse would be about 1 cm. Such a displacement should be clearly seen on the analogue seismograms. We have carefully analysed the records for ∼12 hr prior to and ∼12 hr after the Sarez-Pamir earthquake and did not find any isolated long-period signal similar to the simulated one.

It is possible that the landslide was weaker than the geological studies suggest. It is even possible that the landslide was too weak to be recorded at all, or that its signal is hidden in the earthquake record. For example, the large Love waves, observed in the Sarez-Pamir earthquake record, could be partly due to the horizontal force from the landslide. To test this possibility, we applied beam forming to the European stations (Fig. 2) to enhance the signal-to-noise ratio. We first align the *P* waves and then apply the *P* wave time delays calculated in the ak135 velocity model corresponding to the theoretical slowness calculated with the epicentre parameters. Following this the slant stack to calculate beam traces for a range of slowness values for the fixed backazimuth was applied. This process allows to separate and identify recorded phases by their slowness. As only two stations had vertical components, we used the EW component of our array, which is close to the radial direction, for the *P* waves. For the *S* waves, we used the NS components as a proxy for SH (see Figs A3 and A4, in the Supporting Information for details). The *P* waves of the Sarez-Pamir earthquake are followed by another signal, which has the slowness of a *P* wave and arrives 120 s after the *P* wave of the earthquake. This signal is more clearly observed on low-pass filtered records (corner period of 20 s), indicating that it might have had a low-frequency source. Its amplitude roughly corresponds to the predicted *P* wave amplitude of the simulated Usoy landslide. A signal with the slowness of a *PP* wave is likewise observed on the waveforms 120 s after the *PP* arrival of the earthquake. A corresponding phase is observed for the SH phase with appropriate timing, although this signal is less clear. The quality of our data does not allow us to make any further statements at this point. However, the possibility of the landslide signal being superposed by the earthquake coda should be considered.

We have modelled the full synthetic waveforms for the Belgian station UCC for our DC source and for a combination of the DC and the landslide (single force) source. The non-filtered waveforms are dominated by the earthquake impulse (Fig. 7a), but the low-pass filtered waveforms (40 s corner period) of the combined source (Fig. 7b) show a slightly better fit to the observed seismograms. The

surface waves of the landslide cause a long-period signal, which is not seen in the DC-source-only synthetics, but which seems to be present in the observed waveforms.

7 DISCUSSION

The instrumental seismic record is only a little longer than 100 yr, that is, shorter than most large earthquake recurrence intervals. In the first half of this period, that is, before the establishment of the World-Wide Standardized Seismograph Network, seismographic instruments were diverse and sometimes not well calibrated and timed. Earthquakes from this period could only be described rudimentarily by hypocentre, origin time and magnitude, which were often plagued with significant uncertainty. This leaves many important earthquakes which have very little information associated with them. We showed that analogue seismic records from the earliest stage of seismological observation, digitized and reanalysed with modern tools can still be an important data source extending our knowledge further into the past. The Sarez-Pamir earthquake is probably still the strongest instrumentally recorded shallow earthquake in the Pamir region, making it a worthwhile target for an in-depth study.

We used digitized seismograms from 13 global stations and seismic bulletins to relocate the epicentre of the earthquake and reestimate its magnitude and depth. Our location agrees well with the one based on macroseismic observations (Ambraseys & Bilham 2012; Bindi *et al.* 2014; Fig. 4), also placing it to the west of Lake Sarez. However, both data sets suffer from a west-sided data bias. For the seismic data, this is due to the prevalence of European stations. Intensity data also cluster west of Lake Sarez, along the populated western Pamir valleys and in particular along the Bartang valley, whereas the high plateau of the eastern Pamir was largely uninhabited during winter and consequently has very few observations (Bindi *et al.* 2014). To estimate the bias due to the event-station geometry and Earth model, we relocated the recent (2015 December 7) Sarez M_w7.2 (GFZ 2015; USGS 2015) earthquake with a similar station-phase set as for the Sarez-Pamir earthquake. The location of this earthquake near the Sarez Lake and its large magnitude make it a proper master event for our analysis. Our relocation places the event some ∼25 km northeast of both USGS and GFZ epicentres (Fig. 4), which is outside the standard error ellipse. However, taking into account that the two agency locations, using a large and quite complete phase data sets, are also more than 20 km apart, and in the absence of ground truth, we consider our relocation result to be relevant. Considering that for the 2015 event timing errors are minimal, uncertainties for the 1911 Sarez-Pamir earthquake epicentre must be assumed to be significantly larger than indicated by its $1 \times \sigma$ error ellipse (Fig. 4). The waveforms of the 1911 Sarez-Pamir and the 2015 master event are very similar (Fig. A6, in the Supporting Information), indicating close epicentres and similar focal mechanisms. Our master event relocation places the 1911 event approximately 70 km west of the 2015 event. Based on our uncertainty considerations, however, we would not rule out that both events were colocated, that is, ruptured the same fault. However, the S-P differential traveltimes for European stations are approximately six seconds less for the 1911 Sarez-Pamir earthquake than for the 2015 master event. Their separation accounts for about four seconds difference and a larger S-P time difference may be explained by an additional difference in depth. The additional two seconds difference in S-P times (making in total six seconds) is consistent with the apparently shallower depth of the master event (11 km, as suggested by GFZ 2015) compared to the 1911 Sarez-Pamir earthquake (∼26 km, determined in this study).

The exact depth of the event remains a rather uncertain parameter for the Sarez-Pamir earthquake, although it clearly seems to be crustal. This is important, because the central Pamir also features significant intermediate depth seismicity (Fig. 1). We compared seismograms of the Sarez-Pamir earthquake and a modern deep earthquake (110 km depth) with a nearby epicentres at two neighbouring German stations (Fig. A5, Supporting Information). The waveforms of the deep earthquake show clear depth phases, which are absent for the Sarez-Pamir earthquake. However, the Sarez-Pamir earthquake features considerably larger surface wave amplitudes. These two facts indicate a shallower source for the Sarez-Pamir earthquake. The depths determined from arrival times and waveform modelling produce a similar result (∼26 km depth), yet with a large uncertainty (14 km standard error for the traveltime solution). The seismogenic thickness of the Pamir crust from well-located seismicity is about 20 km (Schurr *et al.* 2014). It is likely that this is also the depth range that accommodated the 1911 Sarez-Pamir rupture.

We determined several different magnitudes based on amplitude readings and waveform modelling. The body wave magnitude m_B differs slightly (Table A3, Appendix A, Supporting Information) for amplitudes measured on the digitized waveforms (m_B7.3 ± 0.2) compared to the one based on the bulletin information (m_B7.1 ± 0.2). This may be explained by station operators' use of different instrument calibration information compared to the information written in the station books used by us. Similar differences are observed for the surface wave station magnitudes M_S, albeit the small number of surface wave amplitudes in bulletins did not allow a proper magnitude calculation. The M_S determined from the digitized waveforms agrees well with the M_S determined by Ambraseys & Bilham (2012), who had more bulletin amplitudes at hand. Ambraseys & Bilham (2012) also calculated a surface wave magnitude M_s7.4 from surface wave readings of Milne seismograph recordings alone. Intensity-based magnitudes give similar results [M7.2–7.6 using different formulae (e.g. Bindi *et al.* 2014; Ambraseys & Bilham 2012)]. Our M_w of 7.3 based on waveform modelling conforms more to the lower range of estimates. The size of the 1911 Sarez-Pamir earthquake is hence comparable to the 2015 event.

The focal mechanism of the Sarez-Pamir earthquake fits very well into the current deformation pattern of the Pamir interior recorded recently by moderate earthquakes (Schurr *et al.* 2014). These earthquakes mainly exhibit sinistral strike-slip faulting on NNE to NE trending (or their conjugate) planes, in agreement with our mechanism. The mechanism of the 1911 Pamir-Sarez earthquake is also similar to the mechanism of the recent M_w 7.2 2015 event (Fig. 4). It corroborates that this is indeed the dominating mode of deformation for the Pamir at the present day, south of the Pamir thrust system. An M_w 7.3 strike-slip earthquake has a rupture length of ∼100 km (e.g. Blaser *et al.* 2010). There are a few known possibly active faults of this dimension in the region, which comply with the epicentre and its uncertainty. Schurr *et al.* (2014) suggested either the Sarez-Murghab thrust system, a roughly east–west trending fault zone reactivating the Rushan-Pshart suture zone, or the sinistral trans-tensional Sarez-Karakul fault system (Fig. 1). Our source mechanism would only comply with the latter, which in addition shows young (but undated) scarps and microseismicity (Strecker *et al.* 1995; Schurr *et al.* 2014). This also seems to be the fault on which the 2015 event occurred. Although the epicentre

solutions locate the event west of this fault, the uncertainties of the solutions (particularly considering the relocation test for the 2015 earthquake described above) would not eliminate it as the accommodating structure. However, we do not want to rule out that the earthquake occurred on another, unmapped fault. The current seismicity shows several earthquake clusters north and west of Sarez Lake for which available mechanisms all show kinematics similar to the 1911 event, although their rupture dimensions are significantly smaller than the presumed rupture length of the 1911 event. However, one should also consider that the seismicity pattern may not have been stationary during the last 100 yr. A crustal earthquake of this size has probably ruptured to the surface, but no fresh surface scarp has been discovered. On the other hand, the region north and west of Lake Sarez, the Yazgulem and Academy of Science ranges, however, is highly glaciated with some of the highest and most rugged topography in the Pamir, making access for mapping extremely difficult.

The mechanism of the Pamir-Sarez earthquake shows that the event contributes to the east–west extension under north–south compression typical for the active tectonic regime of the western and central Pamir. However, also accommodates horizontal shear. GPS data quantify $\sim$1 cm a^{-1} of sinistral shear between the NNW-moving eastern Pamir and the approximately Tajik depression to the northwest (Ischuk *et al.* 2013). The GPS data set, however, is too sparse to localize this shear. Previous studies have attributed it mainly to the Darvaz fault (Burtman & Molnar 1993). However, the seismicity of the western-central Pamir, including the 1911 Pamir-Sarez earthquake, may indicate that this shear is partly also taken up by the sinistral strike-slip faulting apparently typical for the region. The recent change in deformation from thrusting to sinistral shear and extension may be caused by the arrival and commencing of underthrusting of the northwesternmost extent of the Indian lithosphere under the Pamir. Then, the Pamir-Sarez earthquake may ultimately be the result of the northward propagating plate boundary between India and Asia at depth (Schurr *et al.* 2014; Kufner *et al.* 2016).

We do not know when exactly the Usoy landslide occurred. The timing was guessed to be close to the earthquake based on the oral testimonies of two survivors of Usoy village and the large dust cloud people observed in the region directly after experiencing the shaking. It can only be stated with certainty that the landslide and the earthquake were not more then several hours apart. Investigating the waveforms of stacked European records we have found a long-period signal 140 s after the *P* wave, and following the *PP* wave of the earthquake, which may be attributed to the landslide. In this case the landslide signal is very likely to be obscured by the surface waves of the earthquake. As the historical instruments act as a high-pass filter for the long-period landslide signal, it is hard to distinguish from the surface waves. This could be the reason why waveform inversion of the surface waves did not show the same result as for the body waves.

8 CONCLUSIONS

The 1911 Sarez-Pamir earthquake has been recorded by early analogue seismic stations at regional and teleseismic distances. We collected these seismic records, scanned and digitized them, and produced a unique data set of 26 seismograms from 13 stations worldwide for further analysis. We determined new source parameters based on these seismograms, complementing the previous geological and macroseismic studies.

The earthquake hypocentre was relocated to 38.231°N, 72.157°E and 26 km depth based on newly read and bulletin arrival times and arrival time differences, which agrees well with macroseismic observations. The different earthquake magnitudes we determined—m_B7.3, M_s7.7 and M_w7.3—indicate that the event was slightly smaller than previously assumed, yet still the strongest instrumentally recorded crustal earthquake in the region. For the first time we were able to determine a focal mechanism for this event. Waveform modelling revealed NE striking sinistral strike-slip (or conjugate) faulting in good agreement with the current tectonics of the Pamir interior.

Our study confirms that the major part of the seismic signal of the 1911 Sarez-Pamir event is due to the tectonic earthquake. However, we also found a possible signal that may be due to the slightly delayed rockslide. Modelling its contribution based on the parameters of the rockslide fits the data slightly better than a pure DC source.

ACKNOWLEDGEMENTS

We would like to gratefully thank all the people who helped us to collect the historical seismograms: Manfred Herden, Dr Muzli, Dr Muksin, Prof Dr Torsten Dahm, Marius Kriegerowski, Prof Dr Thomas Meier, Annika Fediuk, Kristin Burmeister, Dr Siegfried Wendt, Pia Buchholz, Dr Joachim Wassermann, Dr Rudolf Widmer-Schnidrig, Marina Lopez Muga, Dr Susana Custodio, Mr Ivo Allegretti and others. Additionally, we are grateful to the EUROSISMOS project and INGV, Rome, and especially we thank Dr Graziano Ferrari, Silvia Fillosa and Matteo Quintiliani for their help with the access to the seismograms and digitizing software.

The authors thank Dr James Dewey and Dr Josep Batllo for their advice and support in historical seismograms collection and analysis. Our grateful thanks are also extended to Tim Sonnemann for providing technical support for this work.

This research has been done in the framework of the PROGRESS project (http://www.earth-in-progress.de/index.35.de.html) and financially supported by the German Federal Ministry of Education and Research.

In this work we have used open source software and would like to gratefully acknowledge: GIMP- ; GMT—The Generic Mapping Tools developed by Paul Wessel and Walter H. F. Smith (Wessel *et al.* 2013); Seismic Handler (seismic waveform analysis tool) developed by Dr Klaus Stammler and Dr Marcus Walther; Pyrocko (a seismology toolbox and library) developed by Dr SH.

We would like to thank Lothar Ratschbacher and an anonymous reviewer for their very constructive comments. James Mechie read the entire manuscript, corrected countless minor and major mistakes and improved the readability of the manuscript significantly.

REFERENCES

Allstadt, K., 2013. Extracting source characteristics and dynamics of the August 2010 Mount Meager landslide from broadband seismograms, *J. geophys. Res.,* **118**(3), 1472–1490.

Ambraseys, N. & Bilham, R., 2012. The Sarez-Pamir earthquake and landslide of 18 February 1911, *Seismol. Res. Lett.,* **83**(2), 294–314.

Batlló, J., Stich, D. & Maciá, R., 2008. Quantitative analysis of early seismograph recordings, in *Historical Seismology, Modern Approaches in Solid Earth Sciences*, pp. 385–402, eds Fréchet, J., Meghraoui, M. & Stucchi, M., Springer.

Bindi, D., Parolai, S., Gómez-Capera, A., Locati, M., Kalmetyeva, Z. & Mikhailova, N., 2014. Locations and magnitudes of earthquakes in central Asia from seismic intensity data, *J. Seismol.,* **18**(1), 1–21.

Blaser, L., Krüger, F., Ohrnberger, M. & Scherbaum, F., 2010. Scaling relations of earthquake source parameter estimates with special focus on subduction environment, *Bull. seism. Soc. Am.,* **100**(6), 2914–2926.

Bormann, P. & Saul, J., 2009. Earthquake magnitude, in *Encyclopedia on Complexity and Systems Science,* pp. 2473–2496, ed. Meyers, R.A., Springer.

Bormann, P., Wendt, S. & DiGiacomo, D., 2013. Seismic sources and source parameters, in *New Manual of Seismological Observatory Practice 2 (NMSOP2),* pp. 1–259, ed. Bormann, P., Deutsches GeoForschungsZentrum GFZ, Potsdam.

Brodsky, E.E., Gordeev, E. & Kanamori, H., 2003. Landslide basal friction as measured by seismic waves, *Geophys. Res. Lett.,* **30**(24), 2236, doi:10.1029/2003GL018485.

Burtman, V.S. & Molnar, P., 1993. Geological and geophysical evidence for deep subduction of continental crust beneath the pamir, *Geol. Soc. Am. Spec. Papers,* **281,** 1–76.

Cadek, O., 1987. Studying earthquake ground motion in Prague from Wiechert seismograph records, *Gerl. Beitr. Geophys.,* **96,** 438–447.

Dewey, J. & Byerly, P., 1969. The early history of seismometry (to 1900), *Bull. seism. Soc. Am.,* **59**(1), 183–227.

Ehlert, R., 1898. Zusammenstellung, Erläuterung und kritische Beurteilung der wichtigsten Seismometer mit besonderer Berücksichtigung ihrer praktischen Verwendbarkeit, *Beitr. z. Geophys.,* **3,** 350–475 (In German).

Ekström, G., Nettles, M. & Dziewónski, A., 2012. The global CMT project 2004–2010: centroid-moment tensors for 13,017 earthquakes, *Phys. Earth planet. Inter.,* **200–201**(0), 1–9.

Fréchet, J. & Rivera, L., 2012. Horizontal pendulum development and the legacy of Ernst von Rebeur-Paschwitz, *J. Seismol.,* **16**(2), 315–343.

Fuchs, K. & Müller, G., 1971. Computation of synthetic seismograms with the reflectivity method and comparison with observations, *Geophys. J. R. astr. Soc.,* **23**(4), 417–433.

Galitzin, B., 1915. On the earthquake of 18th February 1911, *Proc. Imperial Acad. Sci. Ser. VI,* **9**(10), 991–998.

Galitzin, G.B., 1910. *Über einen neuen Seismographen für die Vertikal-Komponente des Bodenbewegung: Von Fürst B. Galitzin (Golicyn),* Buchdr. d. Kais. Akad. d. Wiss. (in German).

GFZ 2015. *GeoForschungsZentrum (GEOFON) Potsdam, Germany*. GeoForschungsZentrum (GEOFON) Potsdam, Germany. Available at: http://geofon.gfz-potsdam.de/eqinfo/event.php?id=gfz2015xxuo, last accessed 15 January 2016.

Grabrovec, D. & Allegretti, I., 1994. On the digitizing of historical seismograms, *Geozika,* **11,** 27–31.

Gutenberg, B. & Richter, C.F., 1954. *Seismicity of the Earth and Associated Phenomena,* 2nd edn, Princeton Univ. Press.

Heimann, S., 2015a. *Fomosto: a tool to manage pre-calculated Green's function stores*. GFZ German Research Center for Geosciences, Helmholtz-Zentrum Potsdam, Germany. Available at: http://emolch.github.io/pyrocko/current/fomosto.html, last accessed 10 April 2015.

Heimann, S., 2015b. *Pyrocko—a seismology toolbox and library*. GFZ German Research Center for Geosciences, Helmholtz-Zentrum Potsdam, Germany. Available at: http://emolch.github.io/pyrocko/, last accessed 10 April 2015.

Ischuk, A., 2006. Usoy natural dam: problem of security (Lake Sarez, Pamir Mountains, Tadjikistan), *Ital. J. Eng. Geol. Environ., Spec. Issue,* 1, 189–192.

Ischuk, A. *et al.*, 2013. Kinematics of the Pamir and Hindu Kush regions from GPS geodesy, *J. geophys. Res.,* **118**(5), 2408–2416.

Jeffreys, H., 1923. The Pamir earthquake of 18 February 1911, in relation to the depths of earthquake foci., *Mon. Not. R. astr. Soc. Geophys. Suppl.,* **1,** 22–31.

Jeffreys, H., 1924. *The Earth,* 1st edn, Cambridge Univ. Press, 278 pp.

Kalmetieva, Z., Mikolaichuk, A., Moldobekov, B., Meleshko, A., Jantaev, M.M. & Zubovich, A.V., 2009. *Atlas of Earthquakes in Kyrgyzstan, Bishkek CAIAG—2009*, p. 75 (Editor-in-chief of English version: Dr. H.B. Havenith).

Karnik, V., Kondorskaya, N.V., Riznitchenko, J.V., Savarensky, E.F., Soloviev, S.L., Shebalin, N.V., Vanek, J. & Zatopek, A., 1962. Standardization of the earthquake magnitude scale, *Stud. Geophys. Geod.,* **6,** 41–48.

Kazakov, N., 2004. *Russian Geologists on Lake Sarez*. A collection of the publications related to the lake Sarez and Usoy avalanche. Available at: http://www.nikzdaru.com/, last accessed 15 April 2015.

Kennett, B.L.N. & Engdahl, E.R., 1991. Traveltimes for global earthquake location and phase identification, *Geophys. J. Int.,* **105**(2), 429–465.

Kimball, S. *et al.*, 2014. *GIMP—GNU Image Manipulation Program,* GIMP is a freely distributed piece of software. Available at: http://www.gimp.org/, last accessed 12 December 2014.

Klotz, O., 1915. Earthquake of February 18, 1911, *Bull. seism. Soc. Am.,* **5**(4), 206–213.

Kondorskaya, N. & Shebalin, N. (chief editors), 1982. *New Catalog of Strong Earthquakes in the U.S.S.R. from Ancient Times Through 1977,* p. 609, Report SE31, World Data Center A for Solid Earth Geophysics. Available at: ftp://ftp.ngdc.noaa.gov/hazards/publications/Wdcse-31.pdf, last accessed 4 August 2015.

Kufner, S.-K. *et al.*, 2016. Deep India meets deep Asia: lithospheric indentation, delamination and break-off under Pamir and Hindu Kush (Central Asia), *Earth planet. Sci. Lett.,* **435,** 171–184.

Kulikova, G. & Krüger, F., 2015. Source process of the 1911 M8.0 Chon-Kemin earthquake: investigation results by analogue seismic records, *Geophys. J. Int.,* **201**(3), 1891–1911.

McComb, H.E. & West, J.C., 1931. *Bulletin of the National Research Council, List of Seismologic Stations of the World,* 2nd edn, no. 82, The National Research Council of The National Academy of Sciences, DC.

Michelini, A., De Simoni, B., Amato, A. & Boschi, E., 2005. Collecting, digitizing, and distributing historical seismological data, *EOS, Trans. Am. geophys. Un.,* **86**(28), 261–266.

Milne, J., 1886. *Earthquakes and Other Earth Movements,* International Scientific Series, D. Appleton and Company.

Mooney, W.D., Laske, G. & Masters, T.G., 1998. CRUST 5.1: a global crustal model at 5° × 5°, *J. geophys. Res.,* **103**(B1), 727–747.

Moretti, L., Mangeney, A., Capdeville, Y., Stutzmann, E., Huggel, C., Schneider, D. & Bouchut, F., 2012. Numerical modelling of the Mount Steller landslide flow history and of the generated long period seismic waves, *Geophys. Res. Lett.,* **39**(16), L16402, doi:10.1029/2012GL052511.

Nikiforov, P.M., 1912. *Bulletin of the Permanent Central Seismic Commission,* St. Petersburg, Russia (in Russian).

Oldham, R.D., 1923. The pamir earthquake of 18th february, 1911, *Q. J. Geol. Soc.,* **79**(1–4), 237–245.

Omori, F., 1899. *Horizontal Pendulums for Registering Mechanically Earthquakes and Other Earth-movements,* Tokyo.

Papyrin, L., 2001. *Sarez Catastrophe Geophysical Forecast,* Science World, pp. 183–194 (in Russian).

Preobrazhenskiy, I.A., 1920. *Usoy Avalanche,* Resolution of the Presence of the Geological Committee, 1915 December 1 (in Russian).

Robinson, A.C., Yin, A., Manning, C.E., Harrison, T.M., Zhang, S.-H. & Wang, X.-F., 2004. Tectonic evolution of the northeastern Pamir: constraints from the northern portion of the Cenozoic Kongur Shan extensional system, western China, *Geol. Soc. Am. Bull.,* **116,** doi:10.1130/B25375.1.

Schneider, F. *et al.*, 2013. Seismic imaging of subducting continental lower crust beneath the Pamir, *Earth planet. Sci. Lett.,* **375,** 101–112.

Schurr, B., Ratschbacher, L., Sippl, C., Gloaguen, R., Yuan, X. & Mechie, J., 2014. Seismotectonics of the Pamir, *Tectonics,* **33**(8), 1501–1518.

Schwab, M. *et al.*, 2004. Assembly of the Pamirs: age and origin of magmatic belts from the southern Tien Shan to the southern Pamirs and their relation to Tibet, *Tectonics,* **23**(4), TC4002, doi:10.1029/2003TC001583.

Schweitzer, J., 2001. Hyposat—an enhanced routine to locate seismic events, *Pure appl. Geophys.,* **158**(1–2), 277–289.

Schweitzer, J., 2012. *HYPOSAT/ HYPOMOD,* User Manual. German Research Center for Geosciences, (GFZ), Potsdam.

Schweitzer, J. & Lee, W., 2003. 88 Old Seismic bulletins to 1920: a collective heritage from early seismologists, in *International Handbook of*

Earthquake and Engineering Seismology, pp. 1665–1723, eds Lee, W.H.K., Kanamori, H., Jennings, P. & Kisslinger, C., Academic Press, International Geophysics.

Semenov, P. & Semenov, V., 1958. *Catalog of Earthquakes Felt on the Territory of Tajikistan for the Period 1865–1940, and 1941–1952 Years,* Academy of Sciences Tadzh.SSR, Stalinabad.

Shpilko, G.A., 1914. *The 1911 Earthquake in Pamirs and its Effects. (Chronological Certificate and Report on the Results of the Pamir Squad Expedition)*. Proceedings of the Imperial Russian Geographical Society (in Russian).

Sippl, C. *et al.*, 2013a. Deep burial of Asian continental crust beneath the Pamir imaged with local earthquake tomography, *Earth planet. Sci. Lett.,* **384,** 165–177.

Sippl, C. *et al.*, 2013b. Geometry of the Pamir-Hindu Kush intermediate-depth earthquake zone from local seismic data, *J. geophy. Res.,* **118**(4), 1438–1457.

Sippl, C., Ratschbacher, L., Schurr, B., Krumbiegel, C., Rui, H., Pingren, L. & Abdybachaev, U., 2014. The 2008 Nura earthquake sequence at the Pamir-Tian Shan collision zone, southern Kyrgyzstan, *Tectonics,* **33**(12), 2382–2399.

Sobel, E.R., Schoenbohm, L.M., Chen, J., Thiede, R., Stockli, D.F., Sudo, M. & Strecker, M.R., 2011. Late Miocene-Pliocene deceleration of dextral slip between Pamir and Tarim: implications for Pamir orogenesis, *Earth planet. Sci. Lett.,* **304**(3–4), 369–378.

Storchak, D.A., Di Giacomo, D., Bondár, I., Engdahl, E.R., Harris, J., Lee, W.H.K., Villaseńor, A. & Bormann, P., 2013. Public release of the ISC–GEM global instrumental earthquake catalogue (1900–2009), *Seism. Res. Lett.,* **84**(5), 810–815.

Strecker, M.R., Frisch, W., Hamburger, M.W., Ratschbacher, L., Semiletkin, S., Samoruyev, A. & Sturchio, N., 1995. Quaternary deformation in the Eastern Pamirs, Tajikistan and Kyrgyzstan, *Tectonics,* **14**(5), 1061–1079.

Stübner, K. *et al.*, 2013a. The giant Shakhdara migmatitic gneiss dome, Pamir, India-Asia collision zone, I: Geometry and kinematics, *Tectonics,* **32,** 948–979.

Stübner, K. *et al.*, 2013b. The giant Shakhdara migmatitic gneiss dome, Pamir, India-Asia collision zone, II: Timing of dome formation, *Tectonics,* **32,** 1–28.

Teshebaeva, K., Sudhaus, H., Echtler, H., Schurr, B. & Roessner, S., 2014. Strain partitioning at the eastern Pamir-Alai revealed through SAR data analysis of the 2008 Nura earthquake, *Geophys. J. Int.,* **198**(2), 760–774.

USGS 2015. *Earthquake Archive Search and URL Builder*. NEIC, National Earthquake Information Center, U.S. Geological Survey, National Center, USA.

Wessel, P., Smith, W. H.F., Scharroo, R., Luis, J. & Wobbe, F., 2013. Generic mapping tools: improved version released, *EOS, Trans. Am. geophys. Un.,* **94**(45), 409–410.

Wiechert, E., 1903. *Theory of Automatic Seismographs*, The Royal Society of Sciences in Göttingen, Berlin (in German).

Wiechert, E., 1904. An astatic higher sensitivity pendulum for mechanical registration of earthquakes, *Beitr. z. Geophys.,* **VI,** 435–450 (in German).

Wood, H.O., 1921. *Bulletin of the National Research Council, A List of Seismologic Stations of the World,* Part 7, No. 15, The National Research Council of The National Academy of Sciences, Washington DC.

Yamada, M., Kumagai, H., Matsushi, Y. & Matsuzawa, T., 2013. Dynamic landslide processes revealed by broadband seismic records, *Geophys. Res. Lett.,* **40**(12), 2998–3002.

Zhao, J. *et al.*, 2015. Model space exploration for determining landslide source history from long-period seismic data, *Pure appl. Geophys.,* **172**(2), 389–413.

Zubovich, A.V. *et al.*, 2010. GPS velocity field for the Tien Shan and surrounding regions, *Tectonics,* **29**(6), TC6014, doi:10.1029/2010TC002772.

SUPPORTING INFORMATION

Additional Supporting Information may be found in the online version of this paper:

APPENDIX A. ADDITIONAL INFORMATION ABOUT THE DATA COLLECTION

Table A1. The list of seismic stations used in this study including the information about each institution, which provided the seismic records and the name of the contact person at the time, when the data were collected.

Table A2. Instrument constants for some of the analogue instruments operating in 1911.

Table A3. The station list with all arrival times for all the phases which were available for the Sarez-Pamir earthquake from the digitized waveforms and both local and teleseismic bulletins. The table also includes distances and azimuths to all the stations, and the amplitude and period values where they were available. If the amplitude and the period columns are empty it means either that the value is not available or, in the case of the waveforms, it means that the waveforms were photographed (microfilms) and the true amplitude can not be recovered due to the lack of information about the photo-camera.

Table A4. The amplitude (Amp) and period (T) values for the surface waves recorded on different stations read from the teleseismic bulletins and from the waveforms. The surface wave magnitudes (last column) are calculated using the Prague-Moscow formula (Karnik *et al.* 1962) for each stations and the average magnitude Ms is presented with one standard deviation.

Figure A1. Misfit functions for rake, strike and dip.

Figure A2. The synthetic seismograms simulated for a landslide source. The landslide was modelled as a combination of single-force sources following Zhao *et al.* (2015) with parameters of the Usoy landslide (Preobrazhenskiy 1920; Ambraseys & Bilham 2012). The seismograms were simulated using the instrument response at the historical seismic station GTT in Germany.

Figure A3. Stacked waveforms for different slownesses and fixed backazimuth, plotted as slowness versus time. The stacking is done for a seismic array of European EW components for the P and PP phases. (a) Unfiltered waveforms. (b) Low-pass (20 seconds) filtered waveforms.

Figure A4. Same as Fig. S3 for *S*-waves.

Figure A5. Comparison of the Sarez-Pamir earthquake waveforms and the waveforms of a modern deep (110 km depth) earthquake, for two seismic stations in Germany located ∼40 km apart. The right side of the picture shows the full waveforms and the left side shows the P phase record and highlights the depth phases.

Figure A6. Waveform overlay of the M_w7.3, 1911 Sarez (black) and M_w7.2, 2015 Tajikistan (red) earthquakes. The waveform amplitudes are normalized (http://gji.oxfordjournals.org/lookup/suppl/doi:10.1093/gji/ggw069/-/DC1).

Please note: Oxford University Press is not responsible for the content or functionality of any supporting materials supplied by the authors. Any queries (other than missing material) should be directed to the corresponding author for the paper.